Photodecomposition of Concentrated Ammonia over Nanometer-sized TiO_2, V-TiO_2, and Pt/V-TiO_2 Photocatalysts

Hyung-Joo Choi, Jun-Sik Kim,† and Misook Kang‡,*

School of Environmental Applied Chemistry, KyungHee University, Yongin, Gyeonggi 449-701, Korea
†Environment and Resources Group, Korea Research Institute of Chemical Technology, Daejeon 305-600, Korea
‡Department of Chemistry, College of Science, Yeungnam University, Gyeongsan, Gyeongbuk 712-749, Korea
**E-mail: mskang@ynu.ac.kr*
Received December 5, 2006

To enhance the photodecomposition of concentrated ammonia into N_2, Pt/V-TiO_2 photocatalysts were prepared using solvothermal and impregnation methods. Nanometer-sized particles of 0.1, 0.5 and 1.0 mol% V-TiO_2 were prepared solvothermally, and then impregnated with 1.0 wt% Pt. The X-ray diffraction (XRD) peaks assigned to V_2O_5 at 30.20 (010) and Pt metal at 39.80 (111) and 46.20 (200) were seen in the 1.0 wt% Pt/10.0 mol% V-TiO_2. The particle size increased in the order: pure TiO_2, V-TiO_2 and Pt/V-TiO_2 after thermal treatment at 500 °C, while their surface areas were in the reverse order. On X-ray photoelectron spectroscopy (XPS), the bands assigned to the $Ti2p_{3/2}$ and $Ti2p_{1/2}$ of Ti^{4-}-O were seen in all the photocatalysts, and the binding energies increased in the order: TiO_2 < Pt/V-TiO_2 < V-TiO_2. The XPS bands assigned to the $V2p_{3/2}$ (517.85, 519.35, and 520.55 eV) and $V2p_{1/2}$ (524.90 eV) in the V^{3+}, V^{4-} and V^{5-} oxides appeared over V-TiO_2, respectively, while the band shifted to a lower binding energy with Pt impregnation. The Pt components of Pt/V-TiO_2 were identified at 71.60, 73.80, 75.00 and 76.90 eV, which were assigned to metallic Pt $4f_{7/2}$, PtO $4f_{7/2}$, PtO_2 $4f_{7/2}$, and PtO $4f_{5/2}$, respectively. The UV-visible absorption band shifted closer towards the visible region of the spectrum in V-TiO_2 than in pure TiO_2 and; surprisingly, the Pt/V-TiO_2 absorbed at all wavelengths from 200 to 800 nm. The addition of vanadium generated a new acid site in the framework of TiO_2, and the medium acidic site increased with Pt impregnation. The NH_3 decomposition increased with the amount of vanadium compared to pure TiO_2, and was enhanced with Pt impregnation. NH_3 decomposition of 100% was attained over 1.0 wt% Pt/1.0 mol% V-TiO_2 after 80 min under illumination with 365 nm light, although about 10% of the ammonia was converted into undesirable NO_2 and NO. Various intermediates, such as NO_2, -NH_2, -NH and NO, were also identified in the Fourier transform infrared (FT-IR) spectra. From the gas chromatography (GC), FT–IR and GC/mass spectroscopy (GC/MS) analyses, partially oxidized NO and NO_2 were found to predominate over V-TiO_2 and pure TiO_2, respectively, while both molecules were reduced over Pt/V-TiO_2.

Key Words : V-TiO_2, Pt/V-TiO_2, NH_3 photodecomposition, NO, NO_2

Introduction

An extensive search is under way to develop advanced chemical, biochemical and physicochemical methods to eliminate hazardous chemicals from both air and water. Many studies have examined the photocatalytic treatment of environmental pollutants using semiconductors, such as TiO_2.[1-3] When a TiO_2 semiconductor absorbs a photon and is promoted to an excited state, an electron is transferred from the valence to the conduction band, where it can function as a reducing moiety, leaving a hole in the valence band that is a strong oxidizing entity. The energy gap between the valence and conduction bands in pure TiO_2 is 3.2 eV; therefore, UV light is necessary to excite electrons on the TiO_2 surface. To activate photocatalysts using longer wavelength UV light, recent research has focused on doping/mixing oxides, such as Fe/TiO_2, Pt/TiO_2, Al/TiO_2, Co/TiO_2, and Zn/TiO_2,[4-7] into the TiO_2 anatase structure to lower the band gap energy. Ammonia is a serious pollutant of wastewater, which causes the eutrophication of rivers and lakes,[8,9] and its odor also has negative effects on humans. The importance of the removal of ammonia has increased, and is treated using biological techniques, adsorption and thermal incineration. Recently, the catalytic decomposition of ammonia in wastewater, using metal-TiO_2 photocatalysts, has attracted much attention.[10-13] Most researchers hope that the all ammonia molecules are transformed into N_2 *via* the photocatalytic redox reaction: $4\ NH_3 + 3\ O_2 \rightarrow 2\ N_2 + 6\ H_2O$. However, it has been reported that when metal-incorporated TiO_2 photocatalysts are used for the decomposition of ammonia, considerable amounts of NO, NO_2 and HNO_3 are formed. Consequently, new photocatalysts are needed to eliminate these NO_x compounds, as they cause secondary contamination. Previously, attempts were made to introduce V-TiO_2 for the photodecomposition of methyl orange, which contains a nitrogen component.[14] The addition of vanadium to the TiO_2 framework was found to improve the photodecomposition of nitrogen compounds compared to pure TiO_2.

The main objective of this study was to enhance the

photocatalytic decomposition of ammonia, with the transformation of NH_3 into N_2. Pure TiO_2, V-TiO_2 and Pt/V-TiO_2 photocatalysts were produced using solvothermal and impregnation methods. To confirm the relationship between the physical properties of the photocatalysts and their catalytic decomposition of NH_3, the three different photocatalyst were analyzed using X-ray diffraction (XRD), X-ray photoelectron spectroscopy (XPS), UV-visible spectra and ammonia temperature-programmed desorption (NH_3-TPD). In addition, the intermediates formed during the decomposition of NH_3 were determined using Fourier transform infrared (FT-IR) spectroscopy and gas chromatography (GC/MS), to establish the mechanism of NH_3 photodecomposition over these photocatalysts.

Experimental Section

The preparation of TiO_2, V-TiO_2, and Pt/V-TiO_2 photocatalysts. TiO_2 and 1.0, 5.0 and 10.0 mol% V-TiO_2 photocatalysts were prepared using a conventional solvothermal method[15] to insert vanadium into the TiO_2 framework, as shown in Figure 1a. To prepare the sol mixture, titanium tetraisopropoxide, TTIP (99.95%, Junsei Chemical, Tokyo, Japan) and vanadium chloride (99.9%, VCl_5; Junsei Chemical) were used as the titanium and vanadium precursors, respectively, with ethanol (Wako Pure Chemical, Osaka, Japan) used as the solvent. To 100 mL of ethanol were added 0.1 mol TTIP and either 1.0, 5.0 or 10.0 mol% VCl_5, with 0.4 mol distilled water then added to cause hydrolysis. The TTIP and VCl_5 were hydrolyzed via the OH group during thermal treatment at 200 °C for 24 h. The resulting yellowish precipitate was washed until the pH = 7.0 and then dried at 100 °C for 24 h. Finally, to remove the impurities on the surface of the photocatalysts, they were heated at 500 °C for 1 h. The prepared TiO_2 and V-TiO_2 were impregnated with a Pt precursor, as shown in Figure 1b. To the TiO_2 and V-TiO_2 powders and ethanol prepared above, 1.0 wt% H_2PtCl_4 (99.9%; Aldrich, Milwaukee, WI, USA) was added. The ethanol was removed by evaporation at 60 °C for 2 h, and the mixture dried, and then calcined at 500 °C for 1 h to obtain the crystallized Pt/V-TiO_2 photocatalyst.

The characterizations of TiO_2, V-TiO_2, and Pt/V-TiO_2 photocatalysts. The synthesized TiO_2, V-TiO_2, and Pt/V-TiO_2 powders were subjected to XRD (model PW 1830; Philips, Amsterdam, The Netherlands), using nickel-filtered Cu$K\alpha$ radiation (30 kV, 30 mA), at 2θ angles from 5 to 70°, with a scan speed and time constant of 10° min^{-1} and 1s, respectively. The sizes and shapes of the TiO_2, V-TiO_2 and Pt/V-TiO_2 particles were observed using scanning electron microscopy (SEM, model JEOL-JSM35CF; Tokyo, Japan), with the power set to 15 kV. UV-visible spectra of the TiO_2, V-TiO_2 and Pt/V-TiO_2 powders were obtained using a Shimadzu MPS-2000 spectrometer (Kyoto, Japan) with a reflectance sphere. The spectral range was from 200 to 800 nm. The Brunauer, Emmett and Teller (BET) surface area and pore size distribution (PSD) of the TiO_2, V-TiO_2 and Pt/V-TiO_2 powders were measured by nitrogen gas adsorption using a continuous flow method; a chromatograph equipped with a thermal conductivity detector (TCD), at liquid-nitrogen temperature, was employed. A mixture of nitrogen and helium was used as the carrier gas with a MicroMetrics Gemini 2375 (Londonderry, NH, USA). The sample was

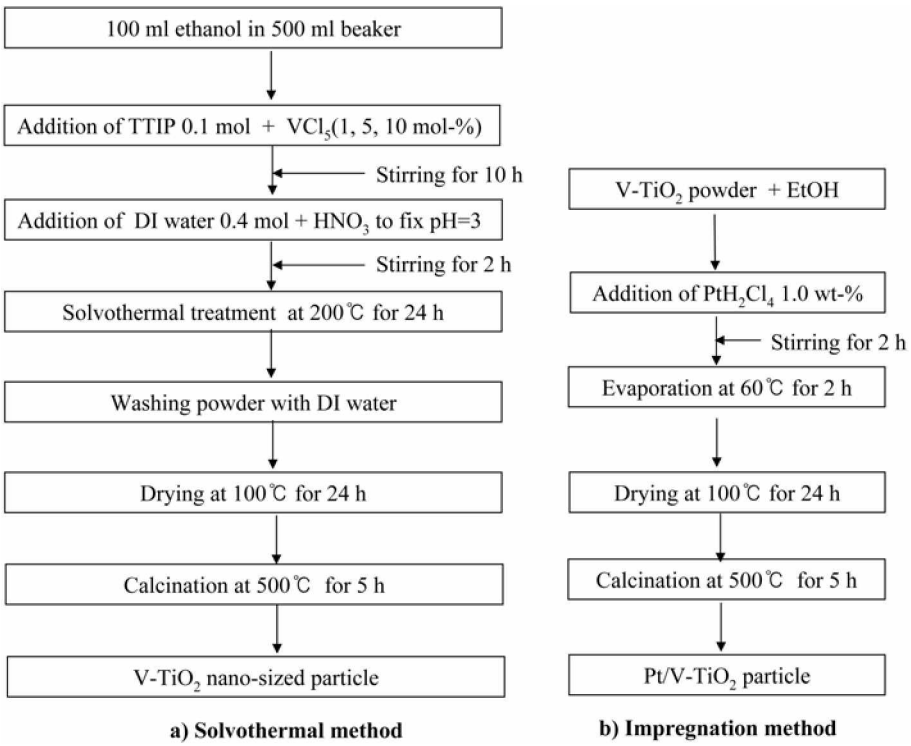

Figure 1. Preparation of nanometer sized TiO_2, V-TiO_2 and Pt/V-TiO_2 photocatalysts using solvothermal and impregnation methods.

treated at 350 °C for 3 h prior to nitrogen adsorption. X-ray photon spectroscopy (XPS) measurements of Pt4f, V2p, Ti2p and O1s were recorded on a ESCA 2000 (VZ Micro-Tech, Oxford, UK) system equipped with a non-monochromatic AlKα (1486.6 eV) X-ray source. The TiO_2, V-TiO_2 and Pt/V-TiO_2 powders were pelletized at 1.2×10^4 kPa for 1 min, and the 1.0-mm pellets then maintained in a vacuum (1.0×10^{-7} Pa) overnight to remove water molecules from the surface prior to measurement. The base pressure of the ESCA system was below 1×10^{-9} Pa. Experiments were recorded with a 200-W source power and an angular acceptance of ± 5°. The analyzer axis was set at an angle of 90° to the specimen surface. Wide scan spectra were measured over a binding energy range of 0 to 1200 eV, with a pass energy of 100.0 eV. The Ar^+ bombardment of the TiO_2, V-TiO_2 and Pt/V-TiO_2 was performed with ion currents between 70 and 100 nA, over an area of 10.0×10.0 mm, with a total sputter time of 2400 s divided into 60 intervals. A Shirley function was used to subtract the background in the XPS data analysis. The XPS signals for O1s, Ti2p, Pt4f and V2p were fitted using mixed Lorentzian-Gaussian curves. NH_3-temperature programmed desorption (TPD) measurements of TiO_2, V-TiO_2 and Pt/V-TiO_2 were carried out on a conventional TPD system equipped with a TCD cell. The catalysts were exposed to He gas at 550 °C for 2 h to remove the water and impurities from the surface. After pretreatment, the samples were exposed to ammonia for 1 h. Finally, programmed heating, at a rate of 10 °C/min, was initiated, to a final temperature of 700 °C. The quantity of desorbed gas was continuously monitored using a TCD cell. About a 3.0 g catalyst sample was loaded into a quartz reactor, heated at 200 °C for 6 h, and then cooled to room temperature under He gas.

Analysis of ammonia decomposition over TiO_2, V-TiO_2, and Pt/V-TiO_2 photocatalysts. Ammonia was decomposed using a gas-phase batch system, as shown in Figure 2a. A quartz cylinder reactor (30 cm long and 1.0 cm in diameter), coupled with UV-lamps (model BBL, 365 nm (or 420 nm), 6 @ 4 W/m^2, 20 cm long × 1.5 cm in diameter; Shinan, Sunchun, Korea) were used for the photoreaction at the specified emitted wavelength, as shown in Figure 2b. The photocatalysts were coated onto 2.0-mm-diameter glass beads as a support, with the quantity of catalyst coating fixed at 1.0 g. The concentration of ammonia added to the batch system was fixed at 1000 ppm. The ammonia concentrations before and after photodecomposition were analyzed using gas chromatography (GC17A; Shimadzu, Kyoto, Japan) with flame-ionization/thermal-conductivity detectors (FID/TCD) (HP-1 capillary column). The percentage ammonia removed was calculated from its disappearance during the decomposition process. All experiments were performed at room temperature and atmospheric pressure. FT-IR spectrometry (FTIR-8400; Shimadzu) and GC/MS were used to quantify the products of ammonia decomposition after a reaction time of 60 min.

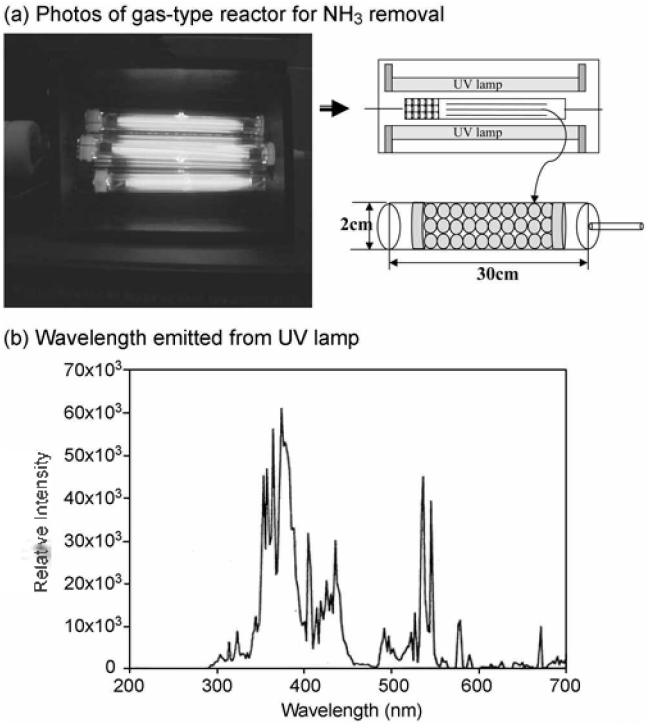

Figure 2. Schematic diagrams of the gas-phase batch reactor for the removal of NH_3 and the wavelengths emitted from the UV-lamp: Reaction conditions: UV-lamp: 4ea (4 W/cm^2, 365 nm or 420 nm), NH_3 1000 ppm, Reaction time: 3 h, Catalyst coated onto glass beads: 1.0 g.

Results and Discussion

Characteristics of the TiO_2, V-TiO_2, and Pt/V-TiO_2 photocatalysts. Figure 3 shows the XRD patterns for the TiO_2, V-TiO_2 and Pt/V-TiO_2 photocatalysts. Photocatalytic TiO_2. All samples had a well-developed anatase structure (symbol A). However, the peak for the anatase structure of Pt/V-TiO_2 was stronger and sharper than those for pure TiO_2 and V-TiO_2. The peaks for V-TiO_2 became rather broader

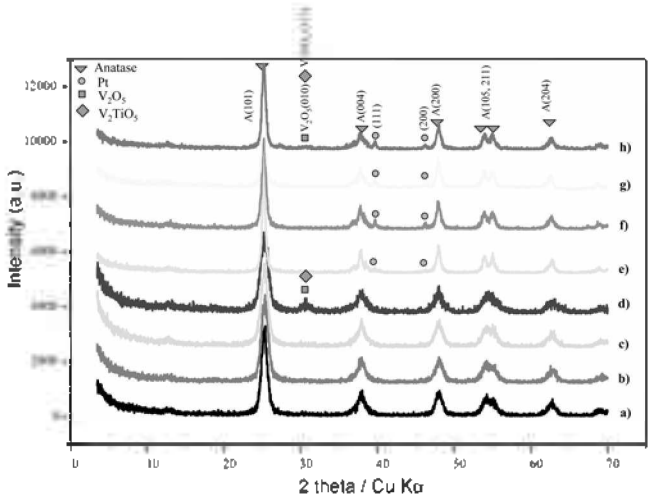

Figure 3. The XRD patterns of the nanometer sized TiO_2, V-TiO_2 and Pt/V-TiO_2 photocatalysts. a) TiO_2, b) V(1.0 mol%)-TiO_2, c) V(5.0 mol%)-TiO_2, d) V(10.0 mol%)-TiO_2, e) Pt(1.0 wt%)/TiO_2, f) Pt(1.0 wt%)/V(1.0 mol%)-TiO_2, and g) Pt(1.0 wt%)/V(5.0 mol%)-TiO_2, h) Pt(1.0 wt%)V(10.0 mol%)-TiO_2.

Table 1. The physical properties of nanometer sized TiO_2, V (5.0 mol%)-TiO_2 and Pt (1.0 wt%)/V (5.0 mol%)-TiO_2 photocatalysts

Catalysts	Composition on surface (Atoms %)				Average pore size (Å)	Average pore volume (cc/g)	Surface area (m^2/g)
	Pt	V	Ti	O			
TiO_2 (500 °C)	–	–	69.21	30.79	158.76	0.71	179.41
V(5.0 mol%)-TiO_2 (500 °C)	–	1.2	27.27	71.53	142.69	0.63	176.89
Pt(1.0 wt%)/V(5.0 mol%)-TiO_2 (500 °C)	0.10	1.57	35.26	63.07	157.52	0.37	95.91

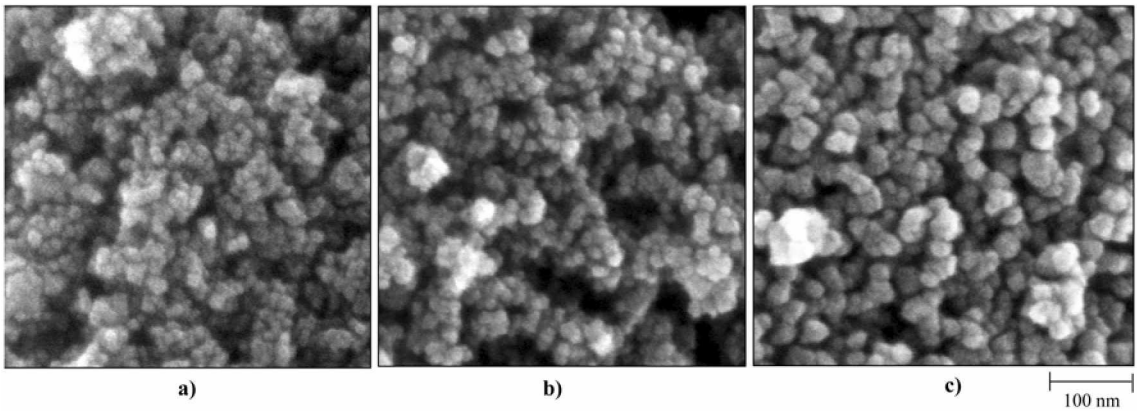

Figure 4. SEM photographs of the nanometer sized TiO_2, V-TiO_2 and Pt/V-TiO_2 photocatalysts. a) TiO_2 (10 nm), b) V(5.0 mol%)-TiO_2 (20 nm), and c) Pt(1.0 wt%)/V(5.0 mol-%)-TiO_2 (30 nm).

with increasing quantity of vanadium. Generally, the broader the peaks, the smaller the crystallites. A peak assigned to V^{5+} (V_2O_5, 101 plane) or V^{3+} (V_2TiO_5, 112 plane) oxide appeared at around $2\theta = 30.20°$ for 10 mol% V-TiO_2, while this peak was not seen for 1.0 and 5.0 mol% V-TiO_2, indicating that the vanadium ions were satisfactorily inserted into the TiO_2 framework up to concentrations of 5.0 mol%. Conversely, the (111) signals assigned to PtO and PtO_2 generally appear at 2θ of 30.00 and 39.76°. Despite our attempts to find these peaks, only two peaks for metallic Pt (111, 200), at $2\theta = 39.80$ and 46.20°, were seen for all the Pt-impregnated samples, although the Pt oxide components could not be determined from the XRD analysis, which may have been due to too the small quantity of Pt components. Scanning electron microscopy (SEM) photographs of TiO_2, 5.0 mol% V-TiO_2, and 1.0 wt% Pt/5.0 mol% V-TiO_2 photocatalysts are shown in Figure 4. All the catalysts were relatively uniform and spherical. The pure TiO_2 particles were the smallest, and the particle size slightly increased with the addition of vanadium, and increased further with platinum impregnation; the sizes in all the catalysts were distributed within the range 20-30 nm. This matched the XRD result shown in Figure 3. Despite platinum impregnation, the Pt/V-TiO_2 particles were still smaller than 30 nm. The particles prepared using the solvothermal method were confirmed to be smaller than those produced using the conventional sol-gel method. Table 1 summarizes the physical properties of the TiO_2, 5.0 mol% V-TiO_2, and 1.0 wt% Pt/5.0 mol% V-TiO_2 photocatalysts. From the energy dispersive analysis of X-rays (EDAX), the true percentage of atomic vanadium/titanium and platinum/vanadium were found to be 4 and 6%, respectively. The increased quantity of platinum compared to that in the sol solution preparation was attributed to the low dispersion of platinum on the surface of V-TiO_2. The bulk pores generated between each nanometer-sized particle ranged between 142 and 159 Å, with pore volumes of 0.37 to 0.71 mL/g. The addition of vanadium did not change the BET (Brunauer, Emmett, and Teller) surface area compared to that of pure TiO_2; however, it was reduced to 95 m^2/g with 1.0 mol% platinum impregnation, since the surface was covered by dispersed platinum. XPS analyses of Ti2p, O1s, V2P and Pt4f were performed on TiO_2, 5.0 mol% V-TiO_2 and 1.0 wt% Pt/5.0 mol% V-TiO_2 particles, as shown in Figure 5. The $Ti2p_{1/2}$ and $Ti2p_{3/2}$ spin-orbital splitting photoelectrons for anatase TiO_2 were located at binding energies of 464.50 and 458.70 eV, respectively, which were assigned to the presence of typical Ti^{4-}, although the band shifted to a higher binding energy for TiO_2. The bands became broader on the addition of vanadium, and markedly shifted to a higher binding energy of 459.10 eV for $Ti2p_{3/2}$ in the V-TiO_2. However, this band was restored on Pt impregnation. In general, a high binding energy indicates that the metal has a high valency. Conversely, the measured FWHM for the $Ti2p_{3/2}$ peak was larger for V-TiO_2 (2.10) than for pure TiO_2 (1.85), but became rather smaller on Pt loading (1.80). In the paper by J.-Z. Hsu *et al.*,[16] the FWHM values were also effective for supposition of the oxidation state of a metal; the larger the FWHM, the higher the oxidation state. Lorentzian-Gaussian curve fitting was used to resolve the O1s peaks at 529.80 and 531.10 eV in the two spectra, which were assigned to metal-O and metal-OH, respectively. The two separate peaks were markedly shifted to higher binding energies, in the order: TiO_2 < Pt/V-TiO_2 < V-TiO_2. Nevertheless, the ratio of metal-O/metal-OH in the O1s peaks were 1.11, 2.52

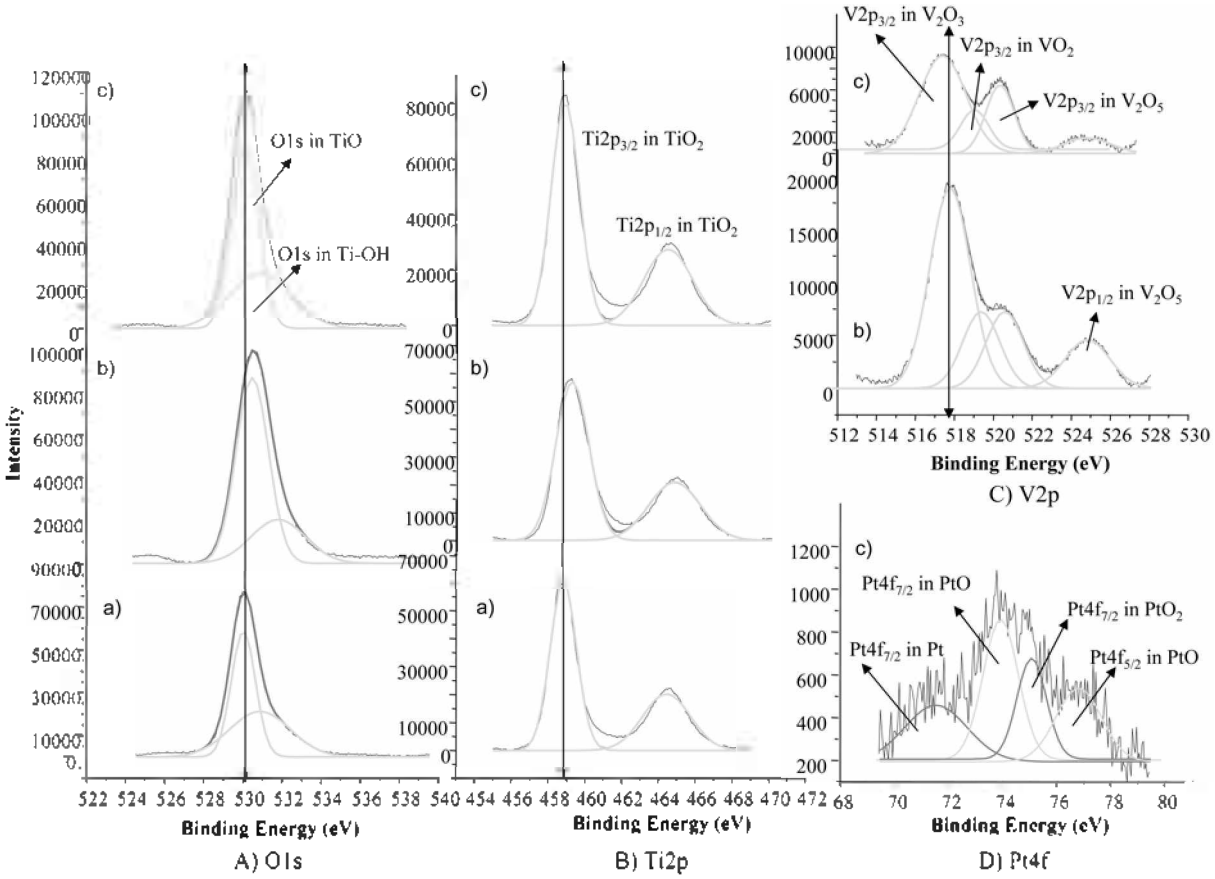

Figure 5. XPS spectra of O1s, Pt4f, Ti2p and V2P, of the nanometer sized TiO_2, V(5.0 mol%)-TiO_2 and Pt (1.0 wt%)/V(5 mol%)-TiO_2 photocatalysts. a) TiO_2, b) V(5.0 mol%)-TiO_2, and c) Pt (1.0 wt%)/V(5 mol%)-TiO_2.

and 1.48 for TiO_2, V-TiO_2 and Pt/V-TiO_2, respectively; a higher metal-OH peak generally indicates that the particles are more hydrophilic.[17,18] In contrast, the FWHM measured for the O1s peak was largest for V-TiO_2, showing a similar tendency for that of the Ti2p peaks. Conversely, the vanadium compounds theoretically have the V^{5+}, V^{4+}, V^{3+} and V^0 oxidation states, and bands assigned to $V2p_{3/2}$ were shown at 516.90, 515.60, 515.20 and 512.40 eV, respectively.[19] In this study, the bands assigned to $V2p_{3/2}$ (517.85, 519.35, and 520.55 eV) and $V2p_{1/2}$ (524.90 eV) for the V^{3+}, V^{4+} and V^{5+} oxides, respectively, appeared over those for V-TiO_2, while these bands shifted to lower binding energies on Pt impregnation, indicating lower metal valence states. Moreover, the FWHM value was larger for Pt/V-TiO_2. The $V2p_{3/2}$ peak areas for V^{3+}(V_2O_3), V^{4+}(VO_2) and V^{5+}(V_2O_5) oxides over those for V-TiO_2 and Pt/V-TiO_2 have ratios of 59.74:15.15:25.11 and 62.51:16.39:21.05, respectively. On the basis of this data, the vanadium components for V-TiO_2 will potentially exist as three oxidation states, but this changed to five oxidation states on Pt loading. This result satisfactorily matched to the XRD result shown in Figure 3. Furthermore, from the XPS results for Ti2p and V2p, the Ti and V ions were confirmed to be reduced on the addition of a platinum component. On the other hand, some papers have determined that the binding energies for the three peaks of Pt4f orbital at 71.2, 72.2 and 73.7 eV belong to the $Pt4f_{7/2}$ of Pt^0, Pt^{2+} and Pt^{4+} oxides, respectively.[20,21] Four peaks were also separated using Lorentzian-Gaussian fitting method for Pt/TiO_2, at 71.6, 73.8, 75.0 and 76.9 eV, assigned to metallic Pt $4f_{7/2}$, PtO $4f_{7/2}$, PtO_2 $4f_{7/2}$ and PtO $4f_{5/2}$, respectively, which were also certified using the Handbook of X-ray photoelectron spectroscopy, published by Perkin-Elmer Corporation.

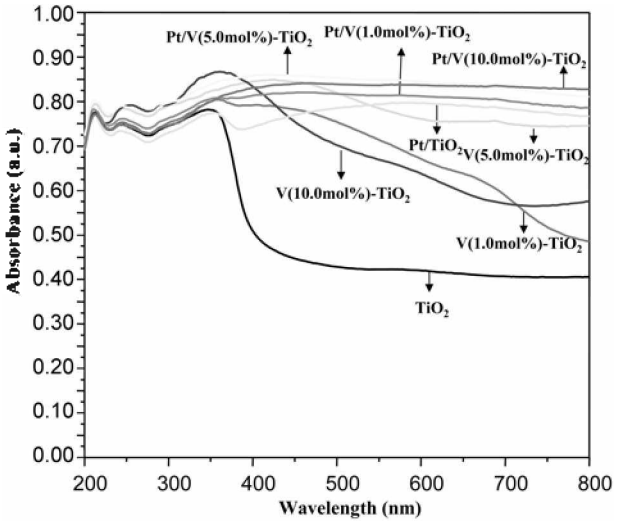

Figure 6. UV-visible spectra of the nanometer sized TiO_2, V-TiO_2 and Pt/V-TiO_2 photocatalysts.

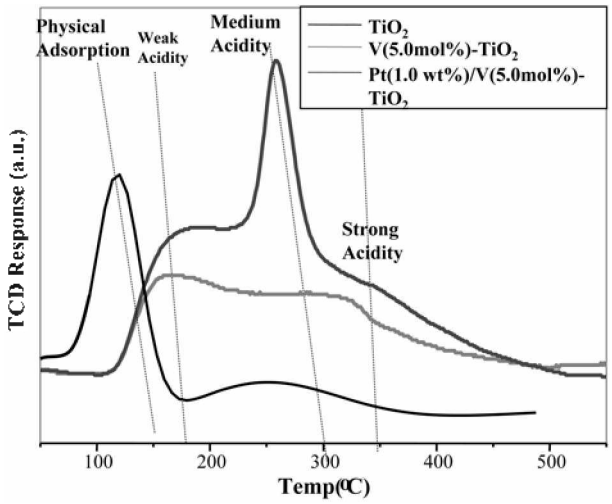

Figure 7. NH_3-TPD profiles of the nanometer sized TiO_2, V(5.0 mol%)-TiO_2 and Pt(1.0 wt%)/V(5 mol%)-TiO_2 photocatalysts.

The ratio of the Pt^0, Pt^{2+} and Pt^{4+} oxides estimated from the $Pt4f_{7/2}$ peak areas was 29.79:40.61:29.59. Therefore, the Pt components for Pt/V-TiO_2 were confirmed to exist as Pt, PtO and PtO_2 in this study; however, the PtO was the most abundant of these components. Figure 6 shows the UV-visible spectra of TiO_2, 5.0 mol% V-TiO_2, and 1.0 wt% Pt/5.0 mol%V-TiO_2 particles. The absorption for the tetrahedral symmetry of Ti^{4+} normally appears around 350 nm. In Figure 6, an absorption band was observed at around 360 nm for pure TiO_2. Moreover, in the spectra for V-TiO_2 and Pt-TiO_2, the absorption bands were shifted to higher wavelengths than for pure TiO_2. Surprisingly, the Pt/V-TiO_2 photocatalysts absorbed at all wavelengths from 200 to 800 nm. Generally, the band gaps in a semiconductor material are closely related to the wave range absorbed. The higher the absorption wavelength, the shorter the band gap. Herein, it is postulated that the addition of a Pt component lowered the band gap energy; consequently, the photocatalysts could be activated by weak energy, such as that provided by visible light. To confirm the effect of the addition of vanadium to the TiO_2 framework, the NH_3-TPD test was performed, the resulting profiles of which is shown in Figure 7. These profiles have two parts: one that appears at temperatures between 100 and 150 °C, which is related to physical adsorption, and the other appears at temperatures between 200 and 400 °C. In general, the low and high temperature peaks corresponded to the weak and strong acid sites, respectively. For pure TiO_2, only one peak assigned to physical adsorption was found at around 100 °C, while a broad peak around 150-350 °C was observed for the V-TiO_2 sample. This indicates that vanadium generated new acid sites on the TiO_2 framework. In addition, a sharp peak appeared at 250 °C when the photocatalyst was impregnated with platinum species, which may be attributable to a special property of platinum.

The decompositions of ammonia over TiO_2, V-TiO_2, and Pt/V-TiO_2 photocatalysts. Figure 8 shows the photocatalytic performances for ammonia removal over the TiO_2, V-TiO_2, and Pt/V-TiO_2 catalysts in a batch photoreactor equipped with UV-radiation at 365 nm. As shown in Figure 8a, 600 ppm of ammonia was removed over pure TiO_2, which was enhanced on the addition of vanadium. Nevertheless, 100 ppm of ammonia remained after 80 min when 5.0 mol% V-TiO_2 was employed, and the ammonia was not completely removed after 160 min. Compared to V-TiO_2, the ammonia decomposition was enhanced with platinum impregnation, and was completely removed after 80 min with the use of 1.0 wt% Pt/10.0 mol% V-TiO_2. It is well known that the deposition of metallic Pt enhances the photocatalytic activity of TiO_2, by increasing of the lifetime of electron-hole pairs, as supported by the present catalysis experiment. From XPS data shown in Figure 5, the metallic Pt was identified as existing on the surface of the Pt/V-TiO_2 catalyst. The photocatalytic performances for ammonia removal under illumination with 420 nm light over the TiO_2, 5.0 mol% V-TiO_2 and 1.0 wt% Pt/5.0 mol%V-TiO_2 catalysts in the batch photoreactor are shown in Figure 9. Compared to the results with 365 nm radiation, as shown in Figure 8, the photocatalytic performances totally decreased in all

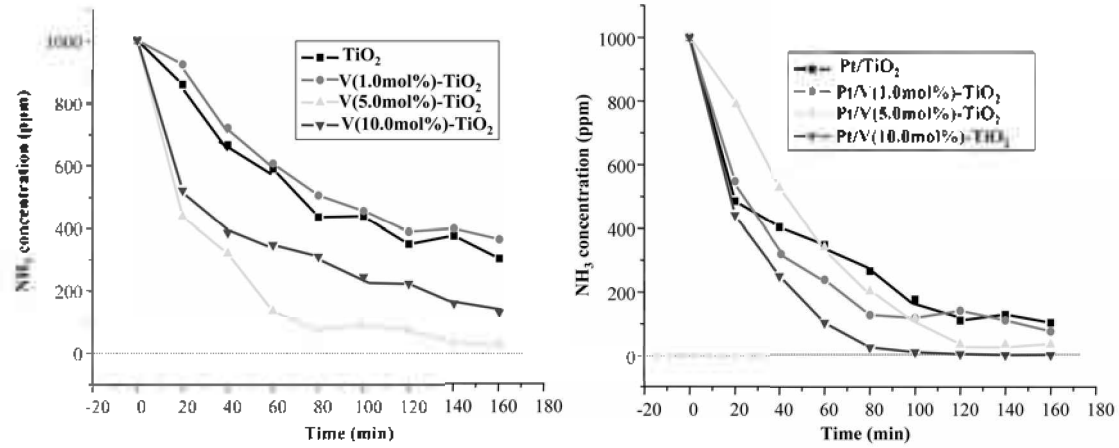

Figure 8. Decomposition of highly concentrated ammonia over the nanometer sized TiO_2, V-TiO_2 and Pt/V-TiO_2 photocatalysts. Reaction conditions: Ammonia concentration, 1000 ppm; Fixed catalyst weight on glass beads, 1.0 g; UV-light intensity, 365 nm; 24 W/m^2; Batch system.

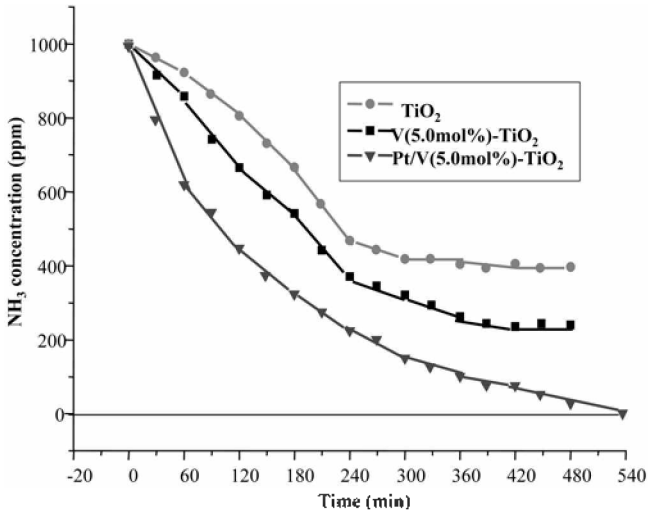

Figure 9. Decomposition of highly concentrated ammonia over the nanometer sized TiO_2, V-TiO_2 and Pt/V-TiO_2 photocatalysts under visible radiation. Reaction conditions: Ammonia concentration, 1000 ppm; Fixed catalyst weight on glass beads, 1.0 g; 420 nm-light; Batch system.

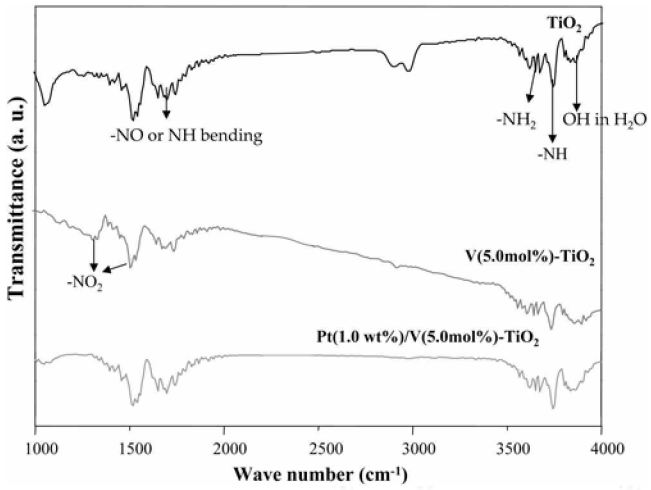

Figure 10. FT-IR spectra obtained during the photocatalytic destruction of ammonia for 1 h over nanometer sized TiO_2, V(5.0 mol%)-TiO_2 and Pt (1.0 wt%) /V(5 mol%)-TiO_2 photocatalysts.

samples. 600 ppm of ammonia was removed over pure TiO_2 after 300 min, and remained unchanged until 480 min. The removal was enhanced about 180 ppm on the addition of vanadium, but the ammonia was not completely removed after 480 min. Compared to pure TiO_2 and V-TiO_2, the ammonia decomposition was enhanced with platinum impregnation, as shown by the results presented in Figure 8, and the ammonia was completely removed by 1.0 wt% Pt/5.0 mol% V-TiO_2 after 540 min. In addition to N_2, however, about 10% of the ammonia was converted into the undesirable NO_2 and NO, which confirmed the platinum-impregnated V-TiO_2 had a greater effect on the photodecomposition of concentrated ammonia. FT-IR analyses were used to determine the products of ammonia photodecomposition after 1 h (Figure 10), which shows the formation of intermediates, such as NO_2, $-NH_2$, -NH and NO. Oxygen or OH radicals, produced from H_2O by UV radiation, were confirmed to react with ammonia, which resulted in the formation

Table 2. Product distributions during the ammonia photo-destruction with reaction time over nanometer-sized TiO_2, V-TiO_2 and Pt/V-TiO_2 photocatalysts

Time (min) \ Catalyst	TiO_2	V(1.0 mol%)-TiO_2	V(5.0 mol%)-TiO_2	V(10.0 mol%)-TiO_2	Pt/V(1.0 mol%)-TiO_2	Pt/V(5.0 mol%)-TiO_2	Pt/V(10.0 mol%)-TiO_2
				NO (ppm)			
20	44	129	57	208	6	7	36
40	20	141	108	238	7	11	46
60	31	195	72	268	8	11	32
80	46	155	61	437	8	7	25
100	29	156	85	261	8	8	21
120	19	136	66	425	8	5	14
140	18	124	43	173	7	6	20
160	17	116	44	177	5	8	19
				NO_2 (ppm)			
20	240	7	–	21	65	36	17
40	98	3	–	26	81	27	15
60	248	8	–	37	81	25	13
80	219	6	–	36	37	18	8
100	226	6	–	32	77	21	6
120	198	6	–	41	60	16	5
140	194	4	–	24	61	15	5
160	171	3	–	29	59	14	5
Total amount of NO+NO_2 after 160 min	188	119	44	206	64	22	24

Initiation Steps	Propagation Steps	Termination Steps
$O_2 \rightarrow 2O\bullet$; $2O\bullet + H_2O \rightarrow 2\,OH\bullet$	3) $\bullet NH_2 + \bullet O \rightarrow NH_2O$	9) $NH_2O + NH_2O \rightarrow N_2 + 2H_2O$
1) $NH_3 + \bullet OH \rightarrow NH_4O\bullet \rightarrow \bullet NH_2 + H_2O$	4) $\bullet NH + \bullet O \rightarrow NHO$	10) $NHO + NHO \rightarrow N_2O + H_2O$
	5) $\bullet NH_2 + \bullet OH \rightarrow NH_3O + \bullet OH \rightarrow \bullet N + 2H_2O$	11) $\bullet NO + \bullet NO \rightarrow N_2 + O_2$
2) $NH_3 + \bullet O \rightarrow NH_3O\bullet \rightarrow \bullet NH + H_2O$	6) $\bullet NH_2 + \bullet OH \rightarrow NH_3O + \bullet O \rightarrow NHO\bullet + H_2O$	12) $\bullet N + \bullet O \rightarrow NO$
	7) $\bullet NH + \bullet OH \rightarrow NH_2O + \bullet OH \rightarrow NHO\bullet + H_2O$	13) $\bullet NO + \bullet O \rightarrow NO_2$
	8) $\bullet NH + \bullet OH \rightarrow NH_2O + \bullet O \rightarrow \bullet NO + H_2O$	

Scheme 1. Suggested mechanism for NH_3 photo-decomposition over nanometer sized metal-TiO_2 photocatalysts.

of N_2, NO, NO_2 and H_2O through a series of intermediate reactions. Moreover, less undesirable products, NO and NO_2, were produced with the use of Pt/V-TiO_2 compared to pure TiO_2 or V-TiO_2. The total quantities of NO and NO_2 produced were estimated using GC, FT-IR and GC/MS analyses, the results of which are summarized in Table 2. However, no NO_2 was found in this study, which was different to the result obtained in previous work[22]; this suggests N_2O is mainly produced from the photo-oxidation of NH_3 over TiO_2. However; in this study, partially oxidized NO and NO_2 were found to be predominant over V-TiO_2 and pure TiO_2, respectively, while the formation of both molecules decreased over Pt/V-TiO_2. The total ($NO+NO_2$) quantities produced over pure TiO_2, 5.0 mol% V-TiO_2 and 1.0 wt% Pt/5.0 mol% V-TiO_2 were 180, 44, and 22 ppm, respectively.

Conclusions

Based on the GC, FT-IR and GC/MS results, a mechanism for NH_3 photodecomposition over nanometer-sized photocatalysts has been suggested, as shown in Scheme 1, which also considered the mechanism proposed by P. Pichat *et al.*.[22] Two oxygen and hydroxyl radicals are generated on UV-radiation, and these radicals attack NH_3 molecules, which lead to the formation NH_2 and NH radicals (steps 1 and 2). The NH and NH_2 radicals are transformed into NH_2O and NHO molecules (steps 3 and 4), via NHO, NO and N radical (steps 5-8) intermediates. Finally, N_2 is produced by self-formation between two NH_2O molecules and two NO radicals, which are generated in the propagation steps. N_2O is produced *via* self-formation between two NHO molecules; however, the formation of this molecule could not be checked. In addition, NO and NO_2 are generated by the reaction between N, O and NO radicals. Consequently, the nanometer-sized V-TiO_2 photocatalyst was confirmed to be very useful for destroying NH_3, and the quantity of undesirable NO_x molecules was reduced with Pt impregnation.

Acknowledgement. This work was supported by the Korea Research Foundation (KRF-2003-D00014), for which the authors are very grateful.

References

1. Yu, J.; Zhao, X. *Mater. Res. Bull.* **2001**, *36*, 97.
2. Hattori, A.; Kawahara, T.; Suzuki, F.; Tada, H.; Ito, S. *J. Colloid Interf. Sci.* **2000**, *232*, 410.
3. Chen, M.-L.; Bae, J.-S.; Oh, W.-C. *Bull. Korean Chem. Soc.* **2006**, *27*, 1423.
4. Kang, M.; Lee, S.-Y.; Chung, C.-H.; Cho, S. M.; Han, G. Y.; Kim, B.-W.; Yoon, K. J. *J. Photochem. Photobiol. A: Chem.* **2001**, *144*, 185.
5. Kang, M.; Choung, S. J.; Park, J. Y. *Catalysis Today* **2003**, *87*, 87.
6. Jung, O.-J.; Kim, S.-H.; Cheong, K.-H.; Li, W.; Saha, S. I. *Bull. Korean Chem. Soc.* **2003**, *24*, 49.
7. Zhou, G.-W.; Lee, D. K.; Kim, Y. H.; Kim, C. W.; Kang, Y. S. *Bull. Korean Chem. Soc.* **2006**, *27*, 368.
8. Riggan, P. I.; Lockwood, R. N.; Lopez, E. N. *Environ. Sci. Technol.* **1985**, *19*, 971.
9. Son, Y.-H.; Jeon, M.-K.; Ban, J.-Y.; Kang, M.; Choung, S.-J. *J. Ind. Eng. Chem.* **2005**, *11*, 938.
10. Kang, M. *Appl. Catal. B: Environ.* **2002**, *37*, 187.
11. Lee, J. H.; Nam, W. S.; Kang, M.; Han, G. Y.; Kim, M.-S.; Ogino, K.; Miyata, S.; Choung, S.-J. *Appl. Catal. A: General* **2003**, *244*, 49.
12. Park, S.-H.; Lee, S.-C.; Kang, M.; Choung, S.-J. *J. Ind. Eng. Chem.* **2004**, *10*, 972.
13. Yeo, M.-K.; Kang, M. *Water Research* **2006**, *40*, 1906.
14. Kang, M.; Choi, D.-H.; Choung, S.-J. *J. Ind. Eng. Chem.* **2005**, *11*, 240.
15. Kang, M. *J. Mol. Catal.* **2003**, *197*, 173.
16. Wu, N.-L.; Lee, M.-S.; Pon, Z.-J.; Hsu, J.-Z. *J. Photochem. Photobiol. A: Chem.* **2004**, *163*, 277.
17. Liu, Q.; Wu, X.; Wang, B.; Liu, Q. *Mater. Res. Bull.* **2002**, *37*, 2255.
18. Yu, J.; Zhao, X.; Zhao, Q.; Wang, G. *Mater. Chem. Phys.* **2001**, *68*, 253.
19. Silversmit, G.; Depla, D.; Poelman, H.; Marin, G. B.; Gryse, R. D. *J. Electron. Spectrosc.* **2004**, *135*, 167.
20. Li, Q.; Wang, K.; Zhang, S.; Yang, J.; Jin, Z. *J. Mol. Catal. A: Chem.* **2006**, *258*, 83.
21. Tang, Y.; Zhang, L.; Wang, Y.; Zhou, Y.; Gao, Y.; Liu, C.; Xing, W.; Lu, T. *J. Power Sources* **2006**, *162*, 124.
22. Mozzanega, H.; Herrmann, J.-M.; Pichat, P. *J. Phys. Chem.* **1979**, *83*, 2251.